BIOCELL
2022 46(4): 1079-1088

Tech Science Press

IR780 loaded hollow MnO_2 nanoparticles for dual-mode imaging and enhanced photodynamic therapy of oral squamous cell carcinoma

Wei PAN[1,2,3,*]; Ye HE[1]; Mengdong HE[1,2,3]; Fei WANG[1,2,3]; Lihua QIU[1,2,*]

[1] Department of Oral and Maxillofacial Surgery, Stomatological Hospital Affiliated to Chongqing Medical University, Chongqing, 401147, China
[2] Chongqing Municipal Key Laboratory of Oral Biomedical Engineering of Higher Education, Chongqing Medical University, Chongqing, 401147, China
[3] Chongqing Key Laboratory of Ultrasound Molecular Imaging, Chongqing Medical University, Chongqing, 400010, China

Key words: Endogenous oxygen generation, Tumor hypoxia, Multimodal imaging, Photodynamic therapy, Oral squamous cell carcinoma

Abstract: Photodynamic therapy (PDT) has emerged as a novel therapeutic modality for cancer treatment, but its therapeutic efficacy is severely limited by the hypoxic tumor microenvironment (TME). Here we designed an innovative multifunctional nano-platform which consists of a hollow MnO_2 shell and internal photosensitizer IR780. It is not only used for multimodal imaging of oral squamous cell carcinoma (OSCC), but also for adjustment hypoxic TME to enhance cancer treatment. Hollow MnO_2 can promote decomposition of tumor endogenous H_2O_2 to relieve tumor hypoxia, thereby enhancing the effect of photodynamic therapy. Photosensitizer IR780 generates singlet oxygen under laser irradiation to kill tumor cells, playing photodynamic effect, can also act as the contrast agents for photoacoustic and fluorescence multiple imaging, providing potential imaging capability for cancer therapeutic guidance and monitoring. Our research results in this article show that $HMnO_2$-IR780 nanocomposite exhibits good biocompatibility and nontoxicity, strong PA/FL imaging contrast, excellent oxygen production capacity and outstanding photodynamic therapy effect. This finding provides a new idea for multimodal imaging-guided nanotherapy for OSCC.

Introduction

Oral squamous cell carcinoma (OSCC) is one of the most common malignant tumors in the oral and maxillofacial region, comprising 90% of all oral tumors (Li *et al.*, 2020; Ren *et al.*, 2017). It is reported that the global 5-year survival rate of patients with OSCC is less than 60%, due to local recurrence and cervical lymph node metastasis (Shi *et al.*, 2018; Wang *et al.*, 2019; Zhao *et al.*, 2015). Surgery, post-operative adjuvant radiotherapy and chemotherapy are currently the primary clinical treatments for OSCC (Wang *et al.*, 2020b; Xiong *et al.*, 2019; Zhu *et al.*, 2019). However, chemotherapeutic drugs are mostly hydrophobic medicine, with fast blood clearance and lack of targeting to the tumor site, resulting in poor therapeutic effect on OSCC (Zhao *et al.*, 2015). Furthermore, drug resistance caused by long-term chemotherapy will also lead to bad therapeutic efficacy and further lead to treatment failure (Fan *et al.*, 2020). Moreover, patients with OSCC are generally unable to receive ablation surgery because it will seriously damage oral structure and affect oral functions, such as speech, chewing and swallowing (Shi *et al.*, 2018). In view of these facts, exploring more effective treatment strategies to treat OSCC at an early stage is essential to improve survival and life quality of OSCC patients.

Photodynamic therapy (PDT) has gradually gained attention as a recently developed therapy strategy for tumor treatments due to its outstanding merits, including noninvasiveness, high selectivity, and low systemic toxicity as compared to traditional chemotherapy and radiotherapy (Liu *et al.*, 2018; Shao *et al.*, 2020; Sun *et al.*, 2019; Zhang *et al.*, 2018). Due to most of the tumors of OSCC are relatively superficial, the tumor tissues are easy to receive laser irradiation, which is conducive to the application of photodynamic therapy (Li *et al.*, 2020). Hence, it can be seen that PDT has the potential to become an effective alternative therapy for OSCC.

In the PDT process, oxygen is an indispensable substrate for causing cell death. However, the vast majority of tumors

*Address correspondence to: Wei Pan, 2018110849@stu.cqmu.edu.cn; Lihua Qiu, 500082@hospital.qmu.edu.cn
Received: 11 April 2021; Accepted: 07 June 2021

Doi: 10.32604/biocell.2022.016934

are in a hypoxic microenvironment and the oxygen consumption in the PDT process will further reduce the oxygen content of the tumor site, affecting the efficacy and prognosis of PDT, which greatly limits its application (He *et al.*, 2018; Liu *et al.*, 2018; Pan *et al.*, 2019; Shao *et al.*, 2020; Yang *et al.*, 2019). Hence, scientists make attempts on advanced strategies to realize continuous and adequate oxygen supply in tumor tissues, to overcoming the limitations of tumor hypoxia, thereby improving the efficacy of PDT.

Thus far, various strategies have been proposed such as directly delivering oxygen into tumor sites by hemoglobin and perfluorocarbon, generating oxygen upon decomposition of chemicals (such as C_3N_4 and CaO_2) carried by nanomaterials to the tumor site, providing endogenous oxygen by catalyzing Internal H_2O_2 to O_2 (Wang *et al.*, 2020c; Yang *et al.*, 2020; Yang *et al.*, 2018). Due to the high content of H_2O_2 in the tumor microenvironment (TME), among the above methods, the strategy of using nanomaterials as endogenous H_2O_2 catalysts to produce oxygen will show good tumor treatment efficiency (Wang *et al.*, 2020c). In recent years, manganese dioxide (MnO_2) as a unique oxygen-producing substrate, has attracted widespread attention due to its high reactivity and specificity to H_2O_2. MnO_2NPs can function as nanozymes to generate O_2 *in situ* by reacting with undesirable and abundantly available tumor metabolites (H_2O_2 and H^+), meanwhile, could be decomposed to harmless water-soluble Mn^{2+} ions that can be rapidly excreted by hepatic and renal systems, avoiding accumulation of the metal oxide commonly found in other metal-based nanoparticle (NP) systems in the body, leading to the low long-term toxicity and good biosafety. In addition, Mn^{2+} ions can also significantly enhance the contrast of T1 magnetic resonance (MR) imaging, so it can be used as an effective magnetic resonance imaging (MRI) agent for tumor-specific imaging and diagnosis (Cao *et al.*, 2020; Wang *et al.*, 2020a; Yang *et al.*, 2017; Zhu *et al.*, 2020a; Zhu *et al.*, 2020b).

IR780 iodide is a lipophilic dye with maximum absorption at 780 nm, which upon near infrared (NIR) light irradiation can effectively convert light to reactive oxygen species (ROS), thus being a potential agent for application in photodynamic therapy to kill cancer cells (Alves *et al.*, 2018). Compared to indocyanine green (ICG), which had been reported as a widely used photosensitizer, IR780 exhibited better photostability in circulation, higher fluorescence intensity and higher $^1O_2$ quantum yield (Liu *et al.*, 2018; Zhang *et al.*, 2018). Furthermore, it has been reported that IR780 have mitochondria active targeting activity, which could preferentially accumulate at intracellular mitochondria without additional chemical conjugation of target ligands. Mitochondrion, as an indispensable cellular organelle, plays key roles in cell aerobic respiration. Mitochondrial-targeted PDT agents can destroy the biological functions of organelles, not only can inhibit cell respiration in cancer cells, thereby reducing oxygen consumption, but can also cause tumor cell death. Thence, mitochondrial targeting is considered one of the effective strategies to improve the efficacy of photodynamic therapy (Yang *et al.*, 2019; Yang *et al.*, 2020; Zhang *et al.*, 2018). More importantly, due to IR780 has excellent Photoacoustic (PA) imaging and NIR fluorescence imaging (FL) ability, research on nanosystems based on IR780 for cancer diagnosis and guiding tumor treatment, has become a hotspot. Constructing a nanoprobe based on IR780 can combine PA and FL imaging to form a multi-modal imaging platform, which can provide complementary advantages over single imaging methods, thereby helping to guide and monitor the photodynamic therapy process and results (Luo *et al.*, 2020; Qiao *et al.*, 2020; Sheng *et al.*, 2018).

In this study, we loaded a photosensitizer IR780 into hollow mesoporous MnO_2 ($HMnO_2$) nanoshells, we for the first time designed and successfully synthesized $HMnO_2$-IR780 nanoparticles to develop a simple, intelligent platform for TME-responsive generation of oxygen to overcome tumor hypoxia, so as to achieve enhanced photodynamic therapy under the guidance of PA imaging and FL imaging. In this system, silica nanoparticles were used as hard template which mesoporous MnO_2 grew on the surface, and then the silica nanoparticles were removed by gentle etching to obtain hollow mesoporous MnO_2 shells. Then Photosensitizers IR780 can be loaded into this hollow mesoporous $HMnO_2$ nano-platform with high loading capacities ($HMnO_2$-IR780). The $HMnO_2$ shell not only promotes loading and transportation photosensitizers but also can effectively catalyze H_2O_2 into O_2 which subsequently receives the energy transferred by IR780 from lasers to produce ROS for PDT. Owing to the superior photoluminescence and photothermal-conversion capability of IR780, this nanoparticle can also act as a PA and FL imaging contrast agent. We have verified the ability of $HMnO_2$-IR780 to produce oxygen and ROS, as well as the PA and FL imaging effects *in vitro*. To evaluate the potential of $HMnO_2$-IR780 NPs as NIR-triggered PDT treatment systems, *in vitro* cellular localization and phototoxicity effects of MnO_2-based nanoplatform were also detected. As far as we know, it is the first time to combine hollow mesoporous $HMnO_2$ structure with the photosensitizer IR780 for dual-mode imaging guided enhanced photodynamic therapy.

Materials and Methods

Materials

TritonX-100, tetraethyl orthosilicate (TEOS), (3-aminopropyl) triethoxysilane (APTES), cycloethane, n-hexanol, ammonia, anhydrous ethanol, and sodium carbonate (Na_2CO_3) were purchased from Ron Reagent Co., Ltd. (Shanghai, China) Potassium permanganate ($KMnO_4$) were obtained from Sinopharm Chemical Reagent Co., Ltd. (China). IR780 iodide were purchased from Sigma-Aldrich. SOSG reagent was purchased from Invitrogen (Thermo Fisher Scientific).1,1'-dioctadecyl-3,3,3',3'-tetramethylindocarbocyanine perchlorate (DiI) and 2-(4-Amidinophenyl)-6-indolecarbamidinedihydrochloride (DAPI) were bought from Beyotime Technology. Calcein-AM/PI Double Staining Kit were obtained from Dojindo Molecular Technologies (China). Deionized water was obtained from a Millipore water purification system. All other reagents were of analytical grade and used as received without further purification.

Synthesis of $HMnO_2$-IR780 NPs

The $HMnO_2$ nanoparticles were synthesized following the previously reported method. First, Solid silica nanoparticles ($sSiO_2$) were synthesized through inverse microemulsion method. Triton X-100 (53 mL), cyclohexane (225 mL) and

n-Hexanol (54 mL) were added into a 500 mL flask under uniform stirring. Then, ammonia (7.5 mL) and H_2O (10 mL) were immediately added and the mixed solution were stirred for 1 h. After that, TEOS (5 mL) and APTES (1 mL) were mixed and added to the above solution. The mixture was stirred for 24 h at the room temperature. $sSiO_2$ nanoparticles were collected by centrifugation (12000 rpm, 10 min) and washed three times with ethanol and water. The obtained $sSiO_2$ nanoparticles were dispersed in ultrapure water (100 mg, 1 mg/mL). Under ultrasonication, $KMnO_4$ aqueous solution (10 mg/mL, 75 mL) were dropwise added into the above solution, and then the reaction was kept stirring for 6 h (Gao *et al.*, 2019b). The as-prepared mesoporous MnO_2-coated $sSiO_2$ were dissolved in 2M Na_2CO_3 aqueous solution at 60°C for 12 h. The obtained hollow mesoporous MnO_2 nanoshells (H-MnO_2) were centrifuged and washed with water several times. The photosensitizer IR780 (ethanolic solution 5 mg/mL) was loaded into $HMnO_2$ nanoparticles (50 mg), which was sonicated using an ultrasonic probe (Sonics & Materials Inc., USA) at a power of 100 W (5 s on and 5 s off) and for another 4 min at a power of 60 W (5 s on and 5 s off) in an ice bath. The $HMnO_2$-IR780 powder were centrifuged and washed three times with ethanol and water. Finally, the prepared $HMnO_2$-IR780 NPs were stored at 4°C for later use.

Characterization

The morphological characteristics of $HMnO_2$-IR780 NPs was observed by transmission electron microscope (TEM, JEM-2100F, Japan) and light microscope (Olympus CKX41; Canada). The sizes and zeta potentials of nanoparticles were determined by a Malvern particle size meter (Malvern, UK). In order to verify the loading of photosensitizer IR780, we also measured the UV-vis absorption spectrum of each component of $HMnO_2$-IR780 NPs. The UV-vis absorption spectrum of $HMnO_2$, IR780, $HMnO_2$-IR780 was recorded respectively by UV-vis-NIR spectrophotometer (UV-3600, Shimadzu, Japan).

Evaluation of the generation of oxygen

Water, IR780, and $HMnO_2$-IR780 (fixed the concentration of IR780 with 5 μg/mL) were added into 3% H_2O_2 solution (4mL), and then stood still for 3 min to observe the bubble formation of each sample (Zhu *et al.*, 2020a). In order to further quantitatively verify the ability of $HMnO_2$-IR780 nanoparticles as catalysts to trigger the decomposition of H_2O_2 to produce oxygen, a portable dissolved oxygen meter (YSI,550A, Japan) was used to monitor the dissolved oxygen in the solution. Similarly, water, IR780 and $HMnO_2$-IR780 were added to the 3% H_2O_2 solution, and the oxygen concentration of each group was monitored and recorded in real time by YSI550A portable dissolved oxygen meter (Cao *et al.*, 2020).

Detection of singlet oxygen generation

In order to further confirm that the $HMnO_2$ nanostructures could enhance the PDT effect of IR780, the *in vitro* photodynamic properties of $HMnO_2$-IR780 and IR780 were evaluated under the conditions of without 3% w/v H_2O_2 or 3% w/v H_2O_2 (Cao *et al.*, 2020). Singlet oxygen fluorescent probe (SOSG) is a common commercial $^1O_2$ detection kit, which was exerted to detect the production of singlet oxygen by $HMnO_2$-IR780 and IR780 under laser irradiation. In this work, Free IR780 and $HMnO_2$-IR780 with or without H_2O_2 added were incubated with SOSG (10 μM), and then irradiated under 808 nm light at 1 W/cm^2 for 5 min. The generated Singlet Oxygen (SO) was measured by the recovered SOSG fluorescence under 494 nm excitation. The Spectra Max M2 multifunctional microplate reader was used to measure its fluorescence intensity (Zhang *et al.*, 2018).

In vitro PA imaging

To examine the PA performance of $HMnO_2$-IR780 NPs, an agarose gel phantom (3% agar w/v in deionized water) with a hole of 1 cm in diameter was prepared (Qiao *et al.*, 2020). A Vevo LAZR Photoacoustic Imaging System (Visual Sonics Inc., Toronto, Canada) was used to obtain PA images. $HMnO_2$-IR780 NPs suspension at the IR780 concentration of 2 mg/mL was used for PA imaging at different wavelengths scanning from 680 to 970 nm (interval = 5 nm) to detect the maximum absorbance (Zhang *et al.*, 2018). Then, the PA signals of different IR780 concentrations of $HMnO_2$-IR780 NPs (2,1, 0.5, 0.25, and 0.125 mg/mL) were measured at the excitation wavelength of 780 nm and the corresponding PA images were acquired. The quantified PA signal intensity of each image was then analyzed by Vevo LAZR software.

In vitro fluorescence imaging

The fetal bovine serum (FBS) resuspension of $HMnO_2$-IR780 NPs with different IR780 concentrations of (2,1, 0.5, 0.25 mg/mL) were prepared, and 100 μL of each concentration was placed in the hole of a 96-well plate. The Xenogen IVIS Spectrum imaging system (Perkin Elmer, USA) was used to acquire Fluorescence images (excitation wavelength 745 nm, emission wavelength 820 nm). Quantitative fluorescence and bio-luminescence imaging system was used for scanning imaging. The quantified fluorescence signal intensity of each image was then analyzed by the system's own software.

Cell culture

A human tongue squamous cell carcinoma cell line (HN-6) was obtained from Dr. Chen (Chongqing Medical University), and the cells were cultured in Dulbecco's Modified Eagle Medium: Nutrient Mixture F-12 (DMEM/F-12, Gibco-BRL, USA) media with 10% fetal bovine serum (FBS, Australian origin, Gibco) and 1% penicillin-streptomycin and incubated under a 5% CO_2 atmosphere at 37°C. The cells were sub-cultured when the cell growth reached approximately 80%.

Cellular uptake

For the *in vitro* cellular uptake test, HN-6 cells were seeded in laser confocal cell-culture dishes (1×10^5 cells per well) and cultured for 24 h. Then, the old media were replaced with new media without serum including $HMnO_2$-IR780 NPs (stained with DiI, λ excitation/λ emission = 549 nm/565 nm) and incubated for various times (1, 2, and 4 h). After that, the cells were washed three times with phosphate buffer saline (PBS), fixed with 4% paraformaldehyde for 15 min, washed with PBS, and dyed with DAPI (λ excitation/λ emission = 364 nm/454 nm) for another

10 min (Odda *et al.*, 2020). After being rinsed with PBS, the cells were observed by confocal laser scanning microscopy (CLSM) (Nikon A1, Japan).

In vitro photodynamic therapy against cancer cells

To test the photodynamic therapeutic effects of $HMnO_2$-IR780 NPs, HN-6 cells were seeded in laser confocal cell-culture dishes (1×10^5 cells per well) for 24 h. Then these HN-6 cells received various treatments including: control, laser only, $HMnO_2$-IR780 only, $HMnO_2$-IR780+Laser, and IR780+Laser. The $HMnO_2$-IR780 and IR780 were diluted according to the concentration of IR780 to 100 μg/mL. After 4 h coincubation, HN-6 cells were irradiated with an 808 nm laser at (1 W/cm^2) for 5 min. Then, the living cells and dead cells were co-stained with CAM and PI solution for CLSM observation (Luo *et al.*, 2020; Zhang *et al.*, 2018).

Statistical analysis

All data were expressed as mean ± SD. A comparison of different groups was determined using one-way analysis of variance (ANOVA) and a significant difference was assumed at $P \leq 0.05$.

Results and Discussion

Design, synthesis and characterization of $HMnO_2$-IR780 NPs

$HMnO_2$-IR780, a novel tumor microenvironment-responsive nano formulation, was designed for dual-modal imaging-guided photodynamic therapy with mitochondria-targeted property, oxygen self-sufficiency and enhanced PDT efficacy by NIR irradiation. These nanoparticles $HMnO_2$-IR780 can accumulate into the tumors through the typical enhanced permeability and retention (EPR) effect, thereby exerting anti-tumor effects, improving efficacy and reducing systemic side effects (Gao *et al.*, 2019a). After entering the tumor cells, the $HMnO_2$ shell can react with tumor endogenous H_2O_2 to generate O_2 *in situ* through the following reaction: $MnO_2 + H_2O_2 + 2H^+ \rightarrow Mn^{2+} + 2H_2O + O_2\uparrow$ (Pan *et al.*, 2019; Wang *et al.*, 2020a; Yang *et al.*, 2017). The loaded IR780 not only function as the photosensitizers for enhanced PDT, but also act as PA and FL imaging contrast agents. In addition, IR780 can actively target cell mitochondria, which further improves the photocytotoxicity of tumor cells during PDT. Since mitochondria are the main organs of cellular respiration, they are highly sensitive to ROS.

The Fig. 1a shows the procedure for the synthesis of $HMnO_2$-IR780NPs. Firstly, monodispersed solid silica nanoparticles ($sSiO_2$) were synthesized as the hard template, by hydrolyzing the tetraethyl orthosilicate (TEOS). Then, by simply mixing $sSiO_2$ with manganese permanganate ($KMnO_4$), a uniform layer of mesoporous MnO_2 was grown on the surface of freshly prepared silica nanoparticles. And $KMnO_4$ can be reduced by unreacted organosilicon existing on those previously synthesized silica nanoparticles. The hollow mesoporous MnO_2 (H-MnO_2) nanoshells were acquired after incubating MnO_2@SiO_2 nanoparticles with a Na_2CO_3 solution to dissolve silica. At last, the loading of the photosensitizer IR780 in the hollow structure of $HMnO_2$ was sonicated using an ultrasonic probe (Sonics & Materials Inc, USA). Using the above method, $HMnO_2$-IR780 NPs for subsequent experiments were synthesized.

The solution of nanoparticles was dark brown when observed by naked eyes. The optical images of the $HMnO_2$-IR780 NPs demonstrated that they were spherical, uniform in size, and well dispersed in pure water, which enabled them not to gather into a mass and adapt well to the external environment (Fig. 1b). Transmission electron microscope (TEM) images clearly showed the nanoparticles appeared round with numerous surface pores (Figs. 1c and 1d). The zeta potential absolute values of typically 30 mV suggested that the particles are very stable; 10–30 mV indicating relatively stable, and 0–10 mV represented rapid agglutination of particle instability. As measured using a Malvern particle size meter, the average zeta potential of the $HMnO_2$-IR780 NPs was −38.9 ± 0.9 mV (Fig. 1e). Obviously, this shows that $HMnO_2$-IR780 NPs have considerable stability, which is conducive to the later photodynamic function *in vivo*. The average size of NPs is crucial for its accumulation in tumors. Ultrasmall nanoparticles (<10 nm) are quickly filtered by the kidneys, resulting in a reduction in tumor site accumulation and retention, while microparticles (380–780 nm) cannot pass through the endothelium of tumor tissue blood vessels (Liu *et al.*, 2018). As shown in Fig. 1f, the mean diameter of the $HMnO_2$-IR780 NPs was 242.7 ± 22.2 nm, which was suitable size for achieving tumor accumulation by the EPR effect. UV–vis–NIR spectrum (Fig. 1g) showed that $HMnO_2$-IR780 was featured with the characteristic absorption of IR780 at 780 nm, while pure $HMnO_2$ exhibited no such a characteristic absorption peak, suggesting the successful encapsulation of IR780 into the nanoshell.

Detection of O_2 release and ROS

As found in many previous studies, the hypoxic TME is responsible for the limited PDT efficacy for treatment of solid tumors as oxygen is an important element in the process of PDT (Cai *et al.*, 2019; Wang *et al.*, 2018; Zhao *et al.*, 2020c).

Therefore, after adding different concentrations of H-MnO_2-IR780 to the 3% H_2O_2 solution, we tested the ability of H-MnO_2 as a catalyst to trigger the decomposition of H_2O_2 by measuring the dissolved O_2 using an oxygen probe, thereby indirectly verifying the H-MnO_2 enhances the effect of photodynamic. As expected, as shown in Fig. 2A, after standing for 3 min, no obvious bubbles were seen in the IR780 group and the pure water group, while a large number of bubbles were seen in the $HMnO_2$-IR780 group, which verified the catalase-like properties of MnO_2. Fig. 2B more intuitively records the trend of the dissolved oxygen content of the three groups of samples over time. It is not difficult to see from the figure that ionized water or IR780 has no effect on H_2O_2, but $HMnO_2$-IR780 all produce a large amount of O_2 bubbles in a time-dependent manner.

In addition, in order to ensure that the O_2 produced by $HMnO_2$-IR780 catalyzed by H_2O_2 can be converted into $^1O_2$ that can be used for PDT treatment, we use SOSG as a sensitive sensor through the electronic transition with $^1O_2$ to detect the fluorescence intensity of SOSG-EP products. We tested the fluorescence intensity of ROS generated by the same concentration of $HMnO_2$-IR780 and free IR780 under the condition of adding H_2O_2 and without H_2O_2, after receiving laser irradiation (808, 1 W/cm^2, 5 min).

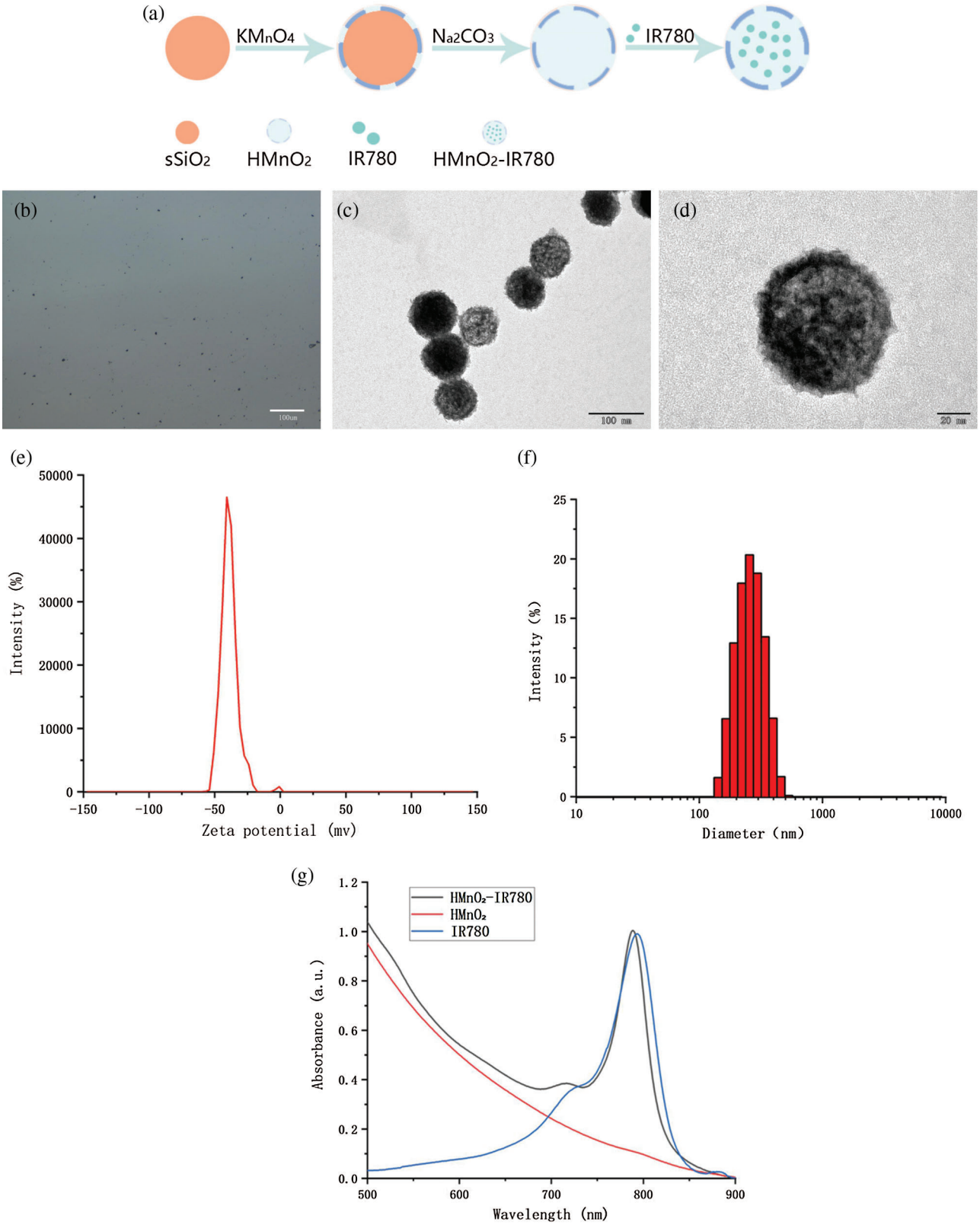

FIGURE 1. (a) Schematic illustration of synthetic procedure of $HMnO_2$-IR780. (b) Optical image of $HMnO_2$-IR780. (c) TEM image of $HMnO_2$-IR780. (d) Enlarged TEM image (scale bar: 20 nm). (e) Zeta potential of $HMnO_2$-IR780. (f) Size distribution of $HMnO_2$-IR780. (g) Absorbance spectra of IR780, $HMnO_2$, $HMnO_2$-IR780 as recorded by UV–vis–NIR spectrophotometer.

As shown in the figure, the ROS level of $HMnO_2$-IR780 is lower than that of free IR780 in the absence of H_2O_2. This may be due to the quenching effect of MnO_2 on IR780 which weakens the photoactivation ability of IR780, so that the content of $^1O_2$ is reduced. weakened. Under the condition of rich H_2O_2, $HMnO_2$-IR780 group, however, due to the O_2 produced by catalyzing H_2O_2 or protons, IR780 can convert O_2 into $^1O_2$ activated by 808 nm laser. As expected, no significant difference was observed in the amount of SO produced by free IR780 under light regardless of the

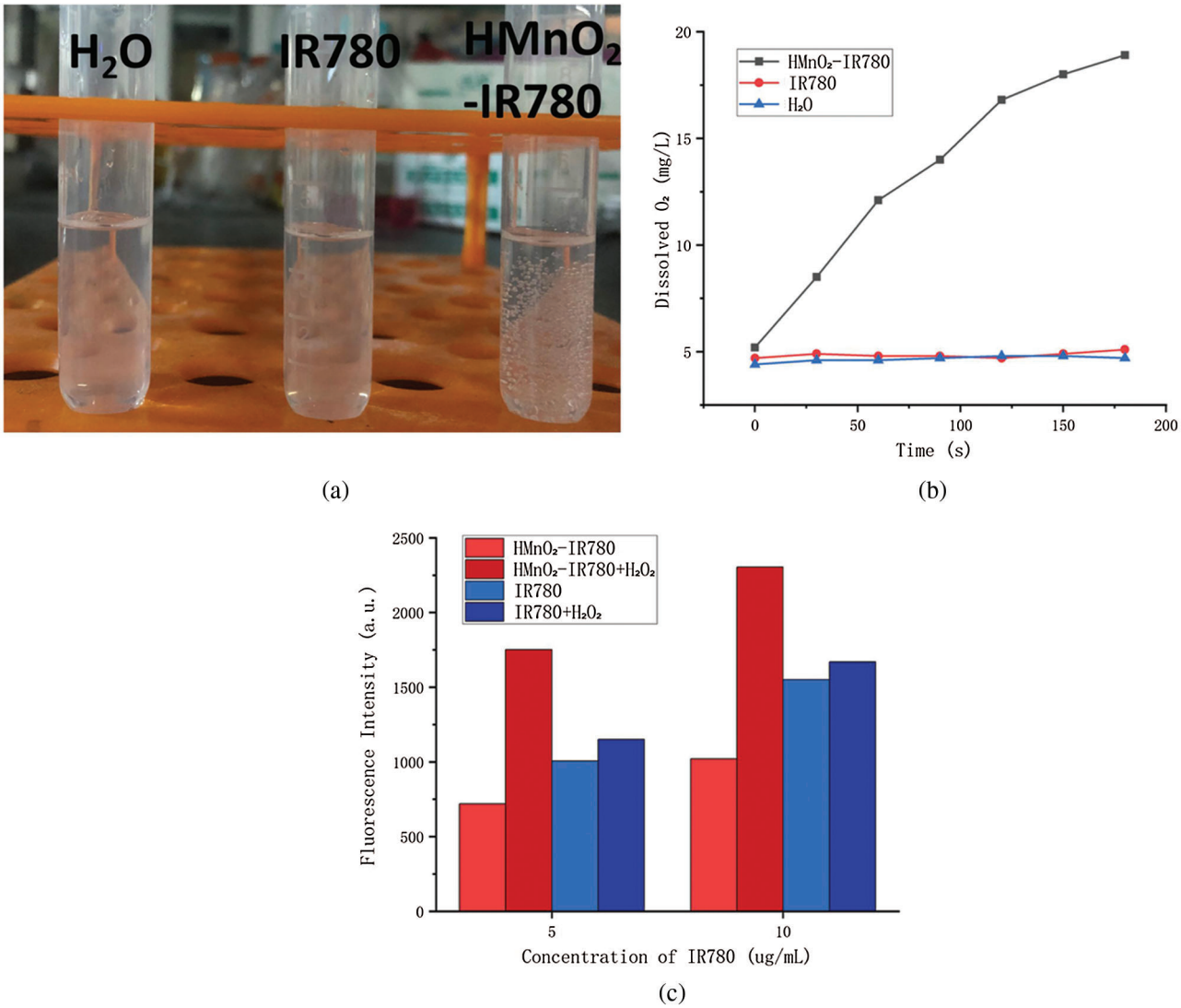

FIGURE 2. (a) The formation of O_2 bubbles in different conditions. (b) Oxygen generation of H_2O, IR780, $HMnO_2$-IR780 measured using dissolved oxygen meter. (c) Singlet oxygen release reflected by SOSG fluorescence in different conditions.

addition of H_2O_2 (100 μM). Therefore, under the condition of low oxygen and high H_2O_2 content of TME, $HMnO_2$-IR780 is expected to be a more effective PDT reagent.

In vitro PA imaging

Photoacoustic (PA) imaging is a rising and noninvasive imaging modality for the diagnosis of tumors, has higher sensitivity and better spatial resolution than CT imaging, holding great potential for clinical applications to visualize the accumulation of nanoprobe and to adjust the therapeutic time window and therapeutic response (Luo *et al.*, 2020; Qiao *et al.*, 2020; Sheng *et al.*, 2018). IR780 iodide is a heptamethine cyanine dye, with a strong optical absorption and emission in the NIR region, is receiving an increasing attention in the area of cancer imaging. Taking into account the outstanding PA imaging capability of IR780, $HMnO_2$-IR780 NPs were expected to be excellent contrast-enhanced agents for clinical application. Consequently, the imaging performance of the NPs was systematically evaluated *in vitro*. Firstly, we performed a full-spectrum scan to detect the imaging window of $HMnO_2$-IR780NPs in PA. After scanned wavelengths from 680 nm to 950 nm at a spectrum interval of 5 nm, it has been seen that the wavelength at 780 nm was the optimal choice for $HMnO_2$-IR780 NPs enhanced PA imaging. Therefore, the PA-imaging performance of $HMnO_2$-IR780 NPs was evaluated at 780 nm. Fig. 3A showed the PA images of $HMnO_2$-IR780 NPs at IR780 concentrations of 0.125, 0.25, 0.5, 1, and 2 mg/mL, which showed a concentration-dependent pattern that as the concentration of nanoparticles increased, the signal of photoacoustic imaging was also stronger. In addition, it is obvious that the signal intensity of photo-acoustic imaging was quite high when the concentration was 2 mg/mL, which verified that $HMnO_2$-IR780 NPs have good photoacoustic imaging ability and revealed that $HMnO_2$-IR780 NPs have the potential to become a photoacoustic contrast agent. And these results were further proofed by quantitative analysis of the corresponding signal intensity. As showed in Fig. 3B, quantitative analysis of the PA imaging signal values of different concentrations of $HMnO_2$-IR780 NPs suggested that it is a linear growth relation.

In vitro FL imaging

Fluorescence imaging is considered to be one of the most promising imaging modalities for diagnostic applications in

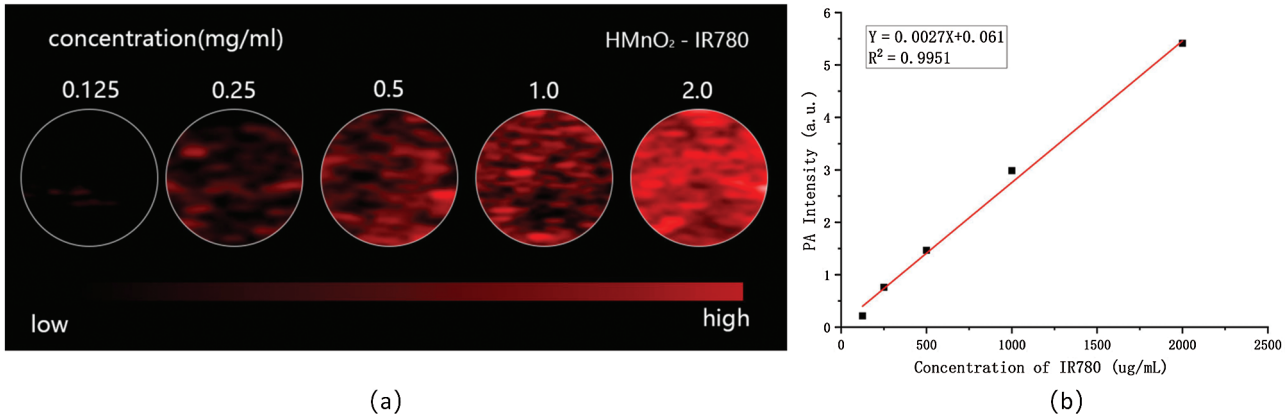

FIGURE 3. (a) *In vitro* PA contrast images of $HMnO_2$-IR780 at different IR780 concentrations. (b) PA values of different concentrations of $HMnO_2$-IR780 NPs.

the clinic due to its able to detect the distribution of nanocontrast agents throughout the body (including tumors) in real time (Chen *et al.*, 2019; Zhao *et al.*, 2020b). The high NIR fluorescence intensity of IR780 in the 807-823 nm wavelength range enlightened us to further verify the performance of $HMnO_2$-IR780 NPs as Fluorescence imaging agents. In addition, according to previous literature reports, the fluorescence intensity of IR780 in different solvents is also different, the fluorescence intensity is the highest in fetal bovine serum, and the lowest in PBS. Then, we tested the fluorescence intensity of $HMnO_2$-IR780 NPs fetal bovine serum resuspension at different concentrations of IR780. Different concentrations of samples were added to 96-well plates. Xenogen IVIS Spectral Imaging system (Perkin Elmer, USA) was used to obtain fluorescence images and collect quantitative fluorescence signal intensity. As we can see in Fig. 4a, the fluorescence signal of the $HMnO_2$-IR780 NPs became stronger as the NP concentration raised from 0.25 to 2 mg/mL, demonstrating that $HMnO_2$-IR780 NP was an effective fluorescent imaging contrast agent.

In summary, the above results show that $HMnO_2$-IR780 NPs is expected to be effective in the treatment of tumors accumulate and act as agents for multimodal imaging. Although PA imaging is capable of displaying functional information of biological tis-sues, for example, it can be used to detect blood vessel distribution and oxygenation status in tumor areas, it remains inapplicable for deep tissue imaging. However, FL imaging is capable to visualize changes in chemical make-up of tissue in real time suiting for wide-field imaging. Consequently, the construction of IR780-based nanoplatform can combine PA imaging and FL imaging together to overcome the limitations of a single imaging mode and provide more accurate and valuable imaging information to adjust the treatment time window and follow-up treatment outcome monitoring.

In vitro cell uptake

The delivery efficiency of $HMnO_2$-IR780 NPs depends on the cellular uptake of $HMnO_2$-IR780 NPs. Therefore, the cellular uptake and accumulation of $HMnO_2$-IR780 NPs in tumor tissues directly affect the treatment efficiency of PDT. The internalization of the $HMnO_2$-based carriers in tumor cells was observed by confocal laser scanning microscopy. First, DiI-stained $HMnO_2$-IR780 NPs was prepared. Then HN-6 cells were co-incubated with DiI-labeled samples for different times. The endocytosis of $HMnO_2$-IR780 NPs was Intuitively observed by CLSM through the fluorescence of the DAPI (blue fluorescence) and DiI (red fluorescence). As shown in Fig. 5, the CLSM image indicated that the cellular uptake of $HMnO_2$-IR780 NPs increased as the culture time increased

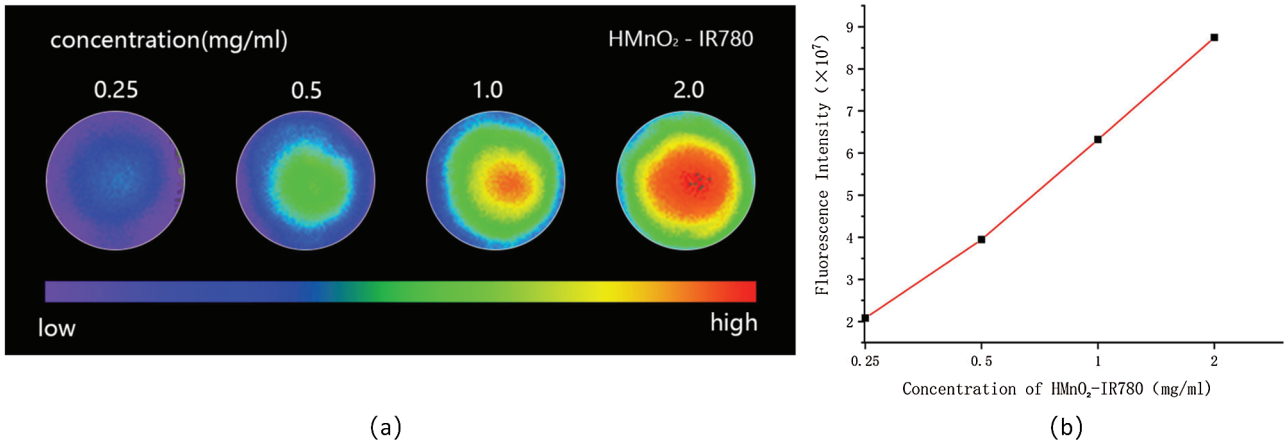

FIGURE 4. (a) *In vitro* NIR fluorescence images of $HMnO_2$-IR780 at different IR780 concentrations. (b) Fluorescence intensities of various concentrations of $HMnO_2$-IR780 NPs.

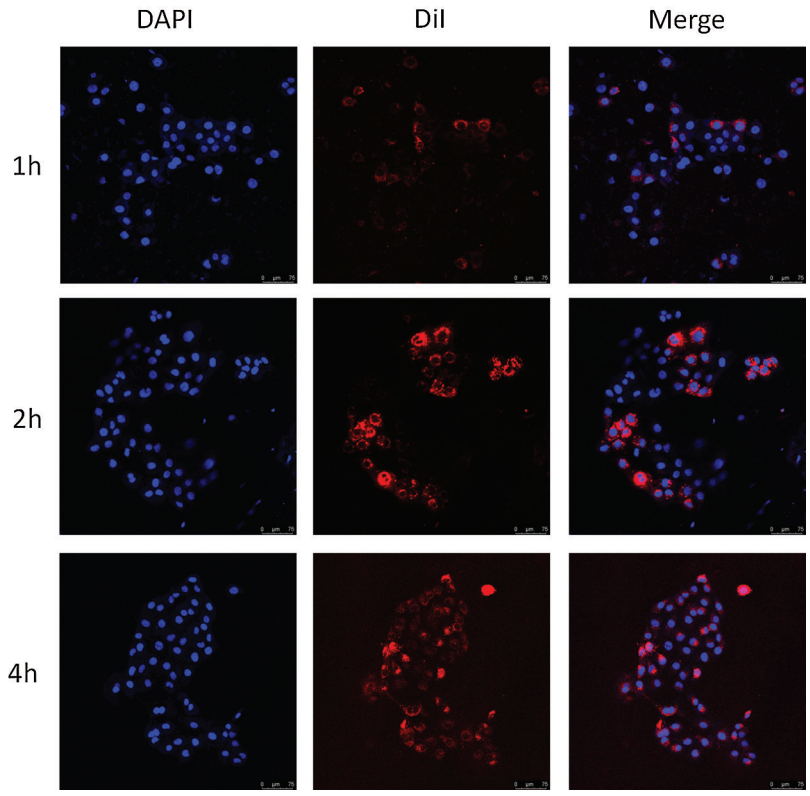

FIGURE 5. Confocal microscopy images (scale bar is 75 μm) of HN-6 cells co-cultured with DiI-labeled $HMnO_2$-IR780 for different times (1, 2, and 4 h). From left column to right column were DAPI-labeled cell nucleus, DiI-labeled NPs and their merged images.

from 1 h to 4 h. In addition, as it was predicted, after 4 h coculture, evident red fluorescence of $HMnO_2$-IR780 (labeled with DiI) was observed in HN-6 cells. According to reports, IR780 has preferential accumulation properties for tumor cells. Cell endocytosis may play a major role in the absorption and accumulation of nano-carriers.

In vitro phototoxicity of $HMnO_2$-IR780 NPs

The mechanism of photodynamic therapy is to activate photosensitizers with specific wavelength of laser light, releasing a large amount of reactive oxygen species (ROS), which can directly kill cancer cells by inducing oxidative damages to lipids, proteins and nucleic acids (Li *et al.*, 2019; Xu *et al.*, 2018; Zhao *et al.*, 2020a). $HMnO_2$-IR780 NPs have the ability to release drugs in response to TME, can up-regulate the level of ROS in tumor cells and destroy the redox cycle in tumor cells, thereby using tumor microenvironment to specifically inhibit tumor cells. This motivates us to further explore the effect and mechanism of enhanced PDT treatment at the cellular level. In order to further study the

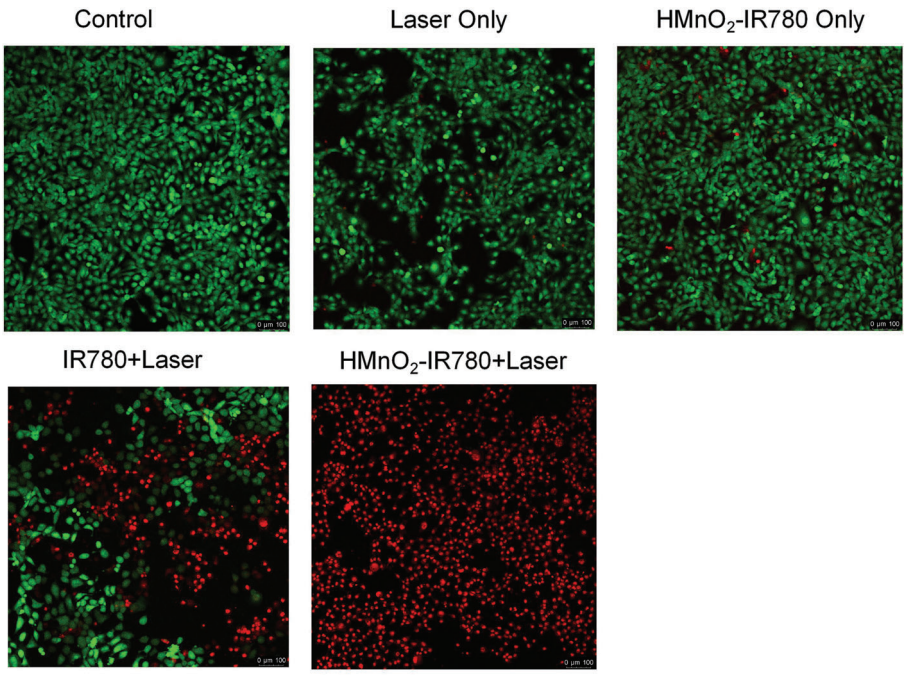

FIGURE 6. Confocal microscopy images (scale bar is 100 μm) of the HN-6 cells after coincubation with $HMnO_2$-IR780 (100 μg/mL) or free IR780 (100 μg/mL) for 4 h followed by various treatments. stained with CAM (live cells are green) and PI (dead cells are red).

therapeutic effect of PDT, a collaborative identification test of calcein acetoxymethyl ester (calcein-AM) and propidium iodide (PI) was carried out, and the corresponding living cells and dead cells were examined by fluorescence under CLSM observation. HN-6 cells were grouped and received different treatments. From Fig. 6 we can intuitively see that green fluorescence of calcein AM and negligible red fluorescence for PI appeared in the control group, laser-only group and $HMnO_2$-IR780 NPs only group, revealing that the 808-laser caused only minor damage and that $HMnO_2$-IR780 NPs had excellent biocompatibility. It is worth noting that even at high concentrations as high as 100 μg/mL, without laser irradiation, $HMnO_2$-IR780 nanoparticles still have no obvious dark toxicity. This show that $HMnO_2$-IR780 nanoparticles are promising nanomedicines for clinical treatment, because good biocompatibility is one of the prerequisites for clinical application of nano-preparations. Moreover, both red fluorescence and green fluorescence were observed in the free IR780+Laser group, showing that photodynamic therapy mediated by photosensitizer IR780 had inhibitory effect on cancer cells to some extent.

Notably, in the $HMnO_2$-IR780+Laser group demonstrated potent photodynamic lethality of $HMnO_2$-IR780 NPs under 808nm laser (1 W/cm^2 5 min). In this group, almost all the cells were stained by PI (red) proving death. The fact that $HMnO_2$-IR780 killed more cells than free IR780 may be due to the increase of IR780 uptake by IR780 encapsulated by $HMnO_2$. In summary, these results reflected the high biocompatible and phototoxicity of $HMnO_2$-IR780 and ensured HN-6 cells could be destroyed completely into death under laser irradiation.

Conclusions

In summary, we have successfully prepared a multifunctional nanoplatform consisting of a IR780-loaded hollow MnO_2 for OSCC photoacoustic and fluorescent molecular imaging guidance/monitoring and oxygen-augmented photodynamic therapy. *In vitro* experiments confirmed that $HMnO_2$-IR780 NPs have a high fluorescence intensity and strong PA signals, demonstrates the potential to become excellent PA/FL contrast agents. Furthermore, $HMnO_2$-IR780 NPs not only improves the stability of IR780 and prolongs its blood circulation, but also decomposes H_2O_2 to produce oxygen, which enhances the effect of photodynamic therapy. *In vitro* cell experiments show that $HMnO_2$-IR780 NPs can be well taken up by cells, and after laser irradiation $HMnO_2$-IR780 NPs can effectively kill HN-6 cells through photodynamic therapy. In conclusion, this study demonstrated a new approach for self-sufficient oxygen-augmented PDT and multiple-imaging guidance/monitoring offering more inspiration to overcome tumor hypoxia and to improve the clinical outcome of OSCC treatment.

Acknowledgement: All synthesis and detection experiments were conducted within the Chongqing Key Laboratory of Ultrasound Molecular Imaging, Chongqing Medical University.

Availability of Data and Materials: The datasets generated during and/or analysed during the current study are available from the corresponding author on reasonable request.

Author Contributions: WP performed the majority of the experiments, including the preparation of nanoparticles, oxygen production experiments, imaging experiments and cell experiments, and wrote the manuscript. YH, MDH and FW analyzed and interpreted the oxygen production experimental data and revised the manuscript. LHQ designed and supervised the study. All authors read and approved the final manuscript.

Funding Statement: The present study was funded by the Chongqing Social Livelihood Science and Technology Innovation Project (Grant No. cstc2016shmszx00010), the Science and Technology Research Project of Chongqing Education Commission (Grant No. KJ1600231) and the Program for Innovation Team Building at Institutions of Higher Education in Chongqing (Grant No. CXTDG201602006).

Conflicts of Interest: The authors declare that they have no conflicts of interest to report regarding the present study.

References

Alves CG, Lima-Sousa R, de Melo-Diogo D, Louro RO, Correia IJ (2018). IR780 based nanomaterials for cancer imaging and photothermal, photodynamic and combinatorial therapies. *International Journal of Pharmaceutics* **542**: 164–175.

Cai X, Xie Z, Ding B, Shao S, Liang S et al. (2019). Monodispersed copper (I)-based nano metal-organic framework as a biodegradable drug carrier with enhanced photodynamic therapy efficacy. *Advanced Science* **6**: 1900848.

Cao W, Liu B, Xia F, Duan M, Hong Y et al. (2020). MnO_2@Ce6-loaded mesenchymal stem cells as an oxygen-laden guided-missile for the enhanced photodynamic therapy on lung cancer. *Nanoscale* **12**: 3090–3102.

Chen C, Sun J, Chen S, Liu Y, Zhu S et al. (2019). A multifunctional-targeted nanoagent for dual-mode image-guided therapeutic effects on ovarian cancer cells. *International Journal of Nanomedicine* **14**: 753.

Fan L, Wang J, Xia C, Zhang Q, Pu Y et al. (2020). Glutathione-sensitive and folate-targeted nanoparticles loaded with paclitaxel to enhance oral squamous cell carcinoma therapy. *Journal of Materials Chemistry B* **8**: 3113–3122.

Gao C, Lin Z, Wang D, Wu Z, Xie H, He Q (2019a). Red blood cell-mimicking micromotor for active photodynamic cancer therapy. *ACS Applied Materials & Interfaces* **11**: 23392–23400.

Gao F, Tang Y, Liu WL, Zou MZ, Huang C et al. (2019b). Intra/extracellular lactic acid exhaustion for synergistic metabolic therapy and immunotherapy of tumors. *Advanced Materials* **31**: 1904639.

He Z, Xiao Y, Zhang JR, Zhang P, Zhu JJ (2018). *In situ* formation of large pore silica-MnO_2 nanocomposites with H^+/H_2O_2 sensitivity for O_2- elevated photodynamic therapy and potential MR imaging. *Chemical Communications* **54**: 2962–2965.

Li M, Li L, Su K, Liu X, Zhang T et al. (2019). Highly effective and noninvasive near-infrared eradication of a Staphylococcus aureus biofilm on implants by a photoresponsive coating within 20 min. *Advanced Science* **6**: 1900599.

Li Q, Zhou R, Xie Y, Li Y, Chen Y, Cai X (2020). Sulphur-doped carbon dots as a highly efficient nano-photodynamic agent against oral squamous cell carcinoma. *Cell Proliferation* **53**: e12786.

Liu WL, Liu T, Zou MZ, Yu WY, Li CX et al. (2018). Aggressive man-made red blood cells for hypoxia-resistant photodynamic therapy. *Advanced Materials* **30**: 1802006.

Luo Y, Qiao B, Zhang P, Yang C, Cao J et al. (2020). TME-activatable theranostic nanoplatform with ATP burning capability for tumor sensitization and synergistic therapy. *Theranostics* **10**: 6987.

Odda AH, Li H, Kumar N, Ullah N, Khan MI et al. (2020). Polydopamine coated PB-MnO_2 nanoparticles as an oxygen generator nanosystem for imaging-guided single-NIR-laser triggered synergistic photodynamic/photothermal therapy. *Bioconjugate Chemistry* **31**: 1474–1485.

Pan W, Ge Y, Yu Z, Zhou P, Cui B et al. (2019). A cancer cell membrane-encapsulated MnO_2 nanoreactor for combined photodynamic-starvation therapy. *Chemical Communications* **55**: 5115–5118.

Qiao B, Luo Y, Cheng HB, Ren J, Cao J et al. (2020). Artificial nanotargeted cells with stable photothermal performance for multimodal imaging-guided tumor-specific therapy. *ACS Nano* **14**: 12652–12667.

Ren S, Cheng X, Chen M, Liu C, Zhao P et al. (2017). Hypotoxic and rapidly metabolic PEG-PCL-C3-ICG nanoparticles for fluorescence-guided photothermal/photodynamic therapy against OSCC. *ACS Applied Materials & Interfaces* **9**: 31509–31518.

Shao Y, Liu B, Di Z, Zhang G, Sun LD et al. (2020). Engineering of upconverted metal-organic frameworks for near-infrared light-triggered combinational photodynamic/chemo-/immunotherapy against hypoxic tumors. *Journal of the American Chemical Society* **142**: 3939–3946.

Sheng D, Liu T, Deng L, Zhang L, Li X et al. (2018). Perfluorooctyl bromide & indocyanine green co-loaded nanoliposomes for enhanced multimodal imaging-guided phototherapy. *Biomaterials* **165**: 1–13.

Shi S, Zhang L, Zhu M, Wan G, Li C et al. (2018). Reactive oxygen species-responsive nanoparticles based on PEGlated prodrug for targeted treatment of oral tongue squamous cell carcinoma by combining photodynamic therapy and chemotherapy. *ACS Applied Materials & Interfaces* **10**: 29260–29272.

Sun Q, Bi H, Wang Z, Li C, Wang C et al. (2019). O_2-generating metal-organic framework-based hydrophobic photosensitizer delivery system for enhanced photodynamic therapy. *ACS Applied Materials & Interfaces* **11**: 36347–36358.

Wang C, Xiao Y, Zhu W, Chu J, Xu J et al. (2020a). Photosensitizer-modified MnO_2 nanoparticles to enhance photodynamic treatment of abscesses and boost immune protection for treated mice. *Small* **16**: 2000589.

Wang D, Shi R, Zhou J, Shi S, Wu H et al. (2018). Photo-enhanced singlet oxygen generation of prussian blue-based nanocatalyst for augmented photodynamic therapy. *Iscience* **9**: 14–26.

Wang F, Wang Z, Pang L, Wan S, Qiu L (2020b). Preparation and *in vitro* study of stromal cell-derived factor 1-targeted Fe_3O_4/poly(lactic-co-glycolic acid)/perfluorohexane nanoparticles. *Experimental and Therapeutic Medicine* **20**: 2003–2012.

Wang J, Sun J, Hu W, Wang Y, Chou T et al. (2020c). A porous Au@Rh bimetallic core-shell nanostructure as an H_2O_2-driven oxygenerator to alleviate tumor hypoxia for simultaneous bimodal imaging and enhanced photodynamic therapy. *Advanced Materials* **32**: 2001862.

Wang Y, Zhang W, Sun P, Cai Y, Xu W et al. (2019). A novel multimodal NIR-II nanoprobe for the detection of metastatic lymph nodes and targeting chemo-photothermal therapy in oral squamous cell carcinoma. *Theranostics* **9**: 391.

Xiong J, Feng J, Qiu L, Gao Z, Li P et al. (2019). SDF-1-loaded PLGA nanoparticles for the targeted photoacoustic imaging and photothermal therapy of metastatic lymph nodes in tongue squamous cell carcinoma. *International Journal of Pharmaceutics* **554**: 93–104.

Xu W, Qian J, Hou G, Wang Y, Wang J et al. (2018). PEGylated hydrazided gold nanorods for pH-triggered chemo/photodynamic/photothermal triple therapy of breast cancer. *Acta Biomaterialia* **82**: 171–183.

Yang G, Xu L, Chao Y, Xu J, Sun X et al. (2017). Hollow MnO_2 as a tumor-microenvironment-responsive biodegradable nano-platform for combination therapy favoring antitumor immune responses. *Nature Communications* **8**: 902.

Yang Z, Wang J, Ai S, Sun J, Mai X, Guan W (2019). Self-generating oxygen enhanced mitochondrion-targeted photodynamic therapy for tumor treatment with hypoxia scavenging. *Theranostics* **9**: 6809.

Yang Z, Wang J, Liu S, Li X, Miao L et al. (2020). Defeating relapsed and refractory malignancies through a nano-enabled mitochondria-mediated respiratory inhibition and damage pathway. *Biomaterials* **229**: 119580.

Yang ZL, Tian W, Wang Q, Zhao Y, Zhang YL et al. (2018). Oxygen-evolving mesoporous organosilica coated prussian blue nanoplatform for highly efficient photodynamic therapy of tumors. *Advanced Science* **5**: 1700847.

Zhang L, Wang D, Yang K, Sheng D, Tan B et al. (2018). Mitochondria-targeted artificial Nano-RBCs for amplified synergistic cancer phototherapy by a single NIR irradiation. *Advanced Science* **5**: 1800049.

Zhao H, Feng H, Liu D, Liu J, Ji N et al. (2015). Self-assembling monomeric nucleoside molecular nanoparticles loaded with 5-FU enhancing therapeutic efficacy against oral cancer. *ACS Nano* **9**: 9638–9651.

Zhao LP, Zheng RR, Chen HQ, Liu LS, Zhao XY et al. (2020a). Self-delivery nanomedicine for O_2 economized photodynamic tumor therapy. *Nano Letters* **20**: 2062–2071.

Zhao XZ, Zhang W, Cao Y, Huang SS, Li YZ et al. (2020b). A cleverly designed novel lipid nanosystem: targeted retention, controlled visual drug release, and cascade amplification therapy for mammary carcinoma *in vitro*. *International Journal of Nanomedicine* **15**: 3953.

Zhao Y, Wang J, Cai X, Ding P, Lv H, Pei R (2020c). Metal-organic frameworks with enhanced photodynamic therapy: Synthesis, erythrocyte membrane camouflage, and aptamer-targeted aggregation. *ACS Applied Materials & Interfaces* **12**: 23697–23706.

Zhu D, Lyu M, Jiang W, Suo M, Huang Q, Li K (2020a). A biomimetic nanozyme/camptothecin hybrid system for synergistically enhanced radiotherapy. *Journal of Materials Chemistry B* **8**: 5312–5319.

Zhu T, Shi L, Yu C, Dong Y, Qiu F et al. (2019). Ferroptosis promotes photodynamic therapy: Supramolecular photosensitizer-inducer nanodrug for enhanced cancer treatment. *Theranostics* **9**: 3293.

Zhu X, Liu Y, Yuan G, Guo X, Cen J et al. (2020b). *In situ* fabrication of MS@MnO_2 hybrid as nanozymes for enhancing ROS-mediated breast cancer therapy. *Nanoscale* **12**: 22317–22329.